

Unveiling pairing anti-halo effect in odd-even staggering in reaction cross sections of weakly bound nuclei

K. Hagino¹ and H. Sagawa²

¹ *Department of Physics, Tohoku University, Sendai, 980-8578, Japan*

² *Center for Mathematics and Physics, University of Aizu, Aizu-Wakamatsu, Fukushima 965-8560, Japan*

We investigate the spatial extension of weakly bound Ne and C isotopes by taking into account the pairing correlation with the Hartree-Fock-Bogoliubov (HFB) method and a 3-body model, respectively. We show that the odd-even staggering in the reaction cross sections of ^{30,31,32}Ne and ^{14,15,16}C are successfully reproduced, and thus the staggering can be attributed to the pairing anti-halo effect. A correlation between a one-neutron separation energy and the anti-halo effect is demonstrated for *s*- and *p*-waves using the HFB wave functions.

PACS numbers: 21.10.Gv,25.60.Dz,21.60.Jz,24.10.-i

Interaction cross sections σ_I and reaction cross sections σ_R of unstable nuclei have been measured using exotic isotope beams produced by projectile fragmentation in high-energy heavy-ion collisions. An important motivation for these studies is to determine the size of unstable nuclei [1–3]. These measurements have in fact discovered the largely extended structure of unstable nuclei such as ¹¹Li [1], ¹¹Be [4], and ^{17,19}C [3]. Nuclei with an extended density distribution are referred to as “halo” nuclei and their structure has been studied extensively as one of the characteristic features of weakly bound nuclei. A proton halo has also been claimed for ⁸B due to a large enhancement of the quadrupole moment [5]. The root-mean-square radius diverges for *s* and *p* waves as the single-particle energy approaches zero [6] and the halo structure can be ascribed to an occupation of an $l = 0$ or $l = 1$ orbit by the valence nucleons near the threshold [7].

Recently, Takechi *et al.* measured the interaction cross sections of neutron-rich Ne isotopes ^{28–32}Ne [8] and reported a halo structure of the ³¹Ne nucleus. The halo structure of ³¹Ne was also reported in the one-neutron removal reaction by Nakamura *et al.* [9]. The interaction cross section σ_I is almost the same as the reaction cross section σ_R for unstable nuclei since the cross sections for inelastic scattering are in general small [10, 11]. In addition to large reaction cross sections for neutron-rich Ne isotopes, the experimental data also show that the reaction cross sections of ³⁰Ne and ³²Ne are quenched as compared to the neighboring odd Ne isotopes, that is, a clear odd-even staggering has been found in the reaction cross sections [8].

In this paper, we discuss the relation between the odd-even staggering in the reaction cross sections and the so called pairing anti-halo effect [12]. The pairing correlation has been known important in nuclei throughout the periodic table, giving an extra binding for paired nucleons [13, 14]. It plays an essential role especially in loosely bound nuclei such as ¹¹Li and ⁶He (so called the Borromean nuclei), because the nuclei will be unbound without the pairing correlations. It is known that many-body correlations strongly modify the pure mean-field picture of loosely bound nuclei. It may happen that the

strong pairing correlations do not allow the decoupling of weakly bound nucleons from the core nucleus and prevent the growth of halo structure. This pairing “anti-halo” effect has been suggested with the Hartree-Fock Bogoliubov (HFB) method [12], but a clear experimental signature of the anti-halo effect has not yet been obtained so far. We will examine in this paper whether the odd-even staggering observed in the recent experimental data for the reaction cross sections of neutron-rich Ne isotopes is an evidence for the pairing anti-halo effect.

In order to address this question, we first study neutron-rich Ne isotopes using the HFB method. The asymptotic behavior of a Hartree-Fock wave function for *s*-wave reads

$$\psi(r) \sim \exp(-\alpha r), \quad (1)$$

where $\alpha = \sqrt{2m|\varepsilon|/\hbar^2}$ with the HF energy ε . The mean square radius of this wave function is then determined as

$$\langle r^2 \rangle_{\text{HF}} = \frac{\int r^2 |\psi(r)|^2 d\mathbf{r}}{\int |\psi(r)|^2 d\mathbf{r}} \propto \frac{1}{\alpha^2} = \frac{\hbar^2}{2m|\varepsilon|}, \quad (2)$$

which will diverge in the limit of vanishing separation energy $|\varepsilon| \rightarrow 0$. This divergence will occur not only for *s*-wave but also for *p*-wave, although the dependence on $|\varepsilon|$ is different [6]. In contrast, the upper component of a HFB wave function, which is relevant to the density distribution, behaves [15]

$$v(r) \propto \exp(-\beta r), \quad (3)$$

where β is proportional to the square root of the quasi-particle energy E ,

$$\beta = \sqrt{\frac{2m}{\hbar^2}(E - \lambda)}, \quad (4)$$

λ being the chemical potential. If we evaluate the quasi-particle energy in the BCS approximation or HFB with canonical basis, it is given as

$$E = \sqrt{(\varepsilon - \lambda)^2 + \Delta^2}, \quad (5)$$

where Δ is the pairing gap. For a weakly bound single-particle state with $\varepsilon \sim 0$ and $\lambda \sim 0$, the asymptotic behavior of the wave function $v(r)$ is therefore determined by the gap parameter as,

$$v(r) \propto \exp\left(-\sqrt{\frac{2m}{\hbar^2}}\Delta \cdot r\right). \quad (6)$$

The radius of the HFB wave function will then be given in the limit of small separation energy $|\varepsilon| \rightarrow 0$ as

$$\langle r^2 \rangle_{\text{HFB}} = \frac{\int r^2 |v(r)|^2 d\mathbf{r}}{\int |v(r)|^2 d\mathbf{r}} \propto \frac{1}{\beta^2} \rightarrow \frac{\hbar^2}{2m\Delta}. \quad (7)$$

As we show, the gap parameter Δ stays finite even in the zero energy limit of ε with a density dependent pairing interaction. Thus the extremely large extension of a halo wave function in the HF field will be reduced substantially by the pairing field and the root-mean-square (rms) radius of the HFB wave function will not diverge. This is called the anti-halo effect due to the pairing correlations [12].

We now numerically carry out mean-field calculations with a Woods-Saxon (WS) potential and also HFB calculations using the single-particle wave functions in the WS potential. As examples of s -wave and p -wave states, we choose the $2s_{1/2}$ state in ^{23}O and $2p_{3/2}$ state in ^{31}Ne , respectively. Although ^{31}Ne is most likely a deformed nucleus[16, 17], for simplicity we assume a spherical Woods-Saxon mean-field potential. Notice that a Woods-Saxon potential with a large diffuseness parameter a yields the $2p_{3/2}$ state which is lower in energy than the $1f_{7/2}$ state, as was shown in Ref. [18]. We use a similar potential with $a=0.75$ fm as in Ref. [18] for ^{31}Ne , while that in Ref. [19] for ^{23}O . For the HFB calculations, we use the density-dependent contact pairing interaction of surface type, in which the parameters are adjusted in order to reproduce the empirical neutron pairing gap for ^{30}Ne [20]. While we fix the Woods-Saxon potential for the mean-field part, the pairing potential is obtained self-consistently with the contact interaction.

The top panel of Fig. 1 shows the mean square radius of the $2s_{1/2}$ state for ^{23}O , while that of Fig. 2 shows the mean square radius of the $2p_{3/2}$ state for ^{31}Ne . In order to investigate the dependence on the single-particle energy, we vary the depth of the Woods-Saxon wells for the $s_{1/2}$ and $p_{3/2}$ states for ^{23}O and ^{31}Ne , respectively. The dashed lines are obtained with the single-particle wave functions, while the solid lines are obtained with the wave function for the canonical basis in the HFB calculations. One can see an extremely large increase of the radius of the WS wave function for both the s -wave and p -wave states in the limit of $\varepsilon_{\text{WS}} \rightarrow 0$. In contrast, the HFB wave functions show only a small increase of radius even in the limit of $\varepsilon_{\text{WS}} \rightarrow 0$. This feature remains the same even when the contribution of the other orbits are taken into account, as shown in the middle panel of Figs. 1 and 2. Due to the pairing effect in the continuum,

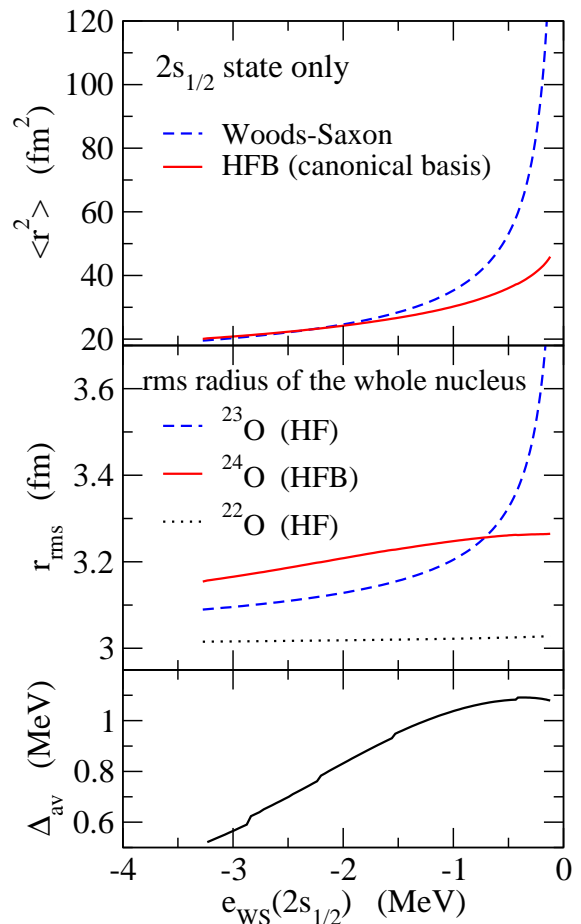


FIG. 1: (Color online) The mean square radii and the average pairing gap as a function of the single particle energy ε_{WS} in a Woods-Saxon mean-field potential. The top panel shows the mean square radius of the $2s_{1/2}$ wave function with and without the pairing correlation, denoted by HFB and Woods-Saxon, respectively. The middle panel shows the rms radii for ^{22}O (the dotted line), ^{23}O (the dashed line), and ^{24}O (the solid line), obtained with the Hartree-Fock (^{22}O and ^{23}O) and the Hartree-Fock-Bogoliubov (^{24}O) calculations. The bottom panel shows the results of the HFB calculations for the average pairing gap of ^{24}O .

the HFB calculations yield a larger radius than the HF calculations for the cases of $\varepsilon_{\text{WS}} \leq -1$ MeV. On the other hand, in the case of $-1 \text{ MeV} < \varepsilon_{\text{WS}} < 0$ MeV the HF wave function (equivalently one quasi-particle wave function in HFB) extends largely, while the HFB wave function does not get much extension due to the pairing anti-halo effect.

In the bottom panel of Figs. 1 and 2, the average pairing gaps are shown as a function of the single particle energy ε_{WS} . It is seen that the average pairing gap increases as ε_{WS} approaches zero. See also Fig. 2 in Ref. [12]. This is due to the fact that the pairing field couples with the extended wave functions of weakly bound nucleons in the self-consistent calculations. That is, the pairing field is extended as the wave functions do and becomes larger for

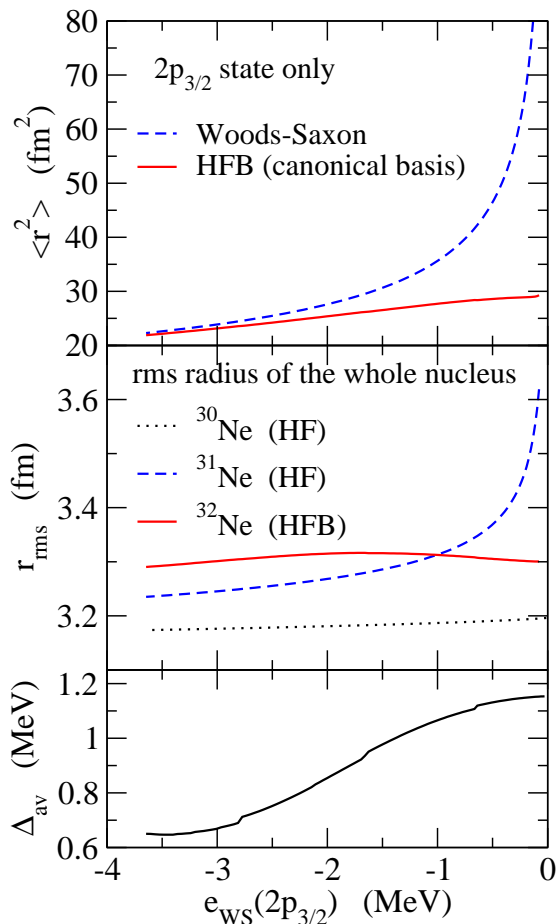


FIG. 2: (Color online) Same as Fig.1, but for the $2p_{3/2}$ state and for $^{30,31,32}\text{Ne}$ isotopes.

a loosely bound system. On the other hand, the pairing gap behaves differently in the non-self-consistent model for the pairing field, in which the pairing field is fixed while solving the HFB equations [21]. In this model, the pairing field has a smaller overlap with the loosely bound nucleons because of the lack of the coupling, leading to a smaller pairing gap in the limit $\epsilon \rightarrow 0$. Thus the anti-halo effect is somewhat underestimated in the non-self-consistent model as is expected from the asymptotic behaviour of the HFB wave function given by Eq. (6).

Let us now calculate the reaction cross sections for the $^{30,31,32}\text{Ne}$ isotopes and discuss the role of pairing anti-halo effect. To this end, we use the Glauber theory, in which we adopt the prescription in Refs. [18, 22] in order to take into account the effect beyond the optical limit approximation. Fig. 3 shows the reaction cross sections of the $^{30,31,32}\text{Ne}$ nuclei on a ^{12}C target at 240 MeV/nucleon. We use the target density given in Ref. [10] and the profile function for the nucleon-nucleon scattering given in Ref. [23]. In order to evaluate the phase shift function, we use the two-dimensional Fourier transform technique [24]. The cross sections σ_R shown in Fig. 3 are calculated by using projectile densities constrained

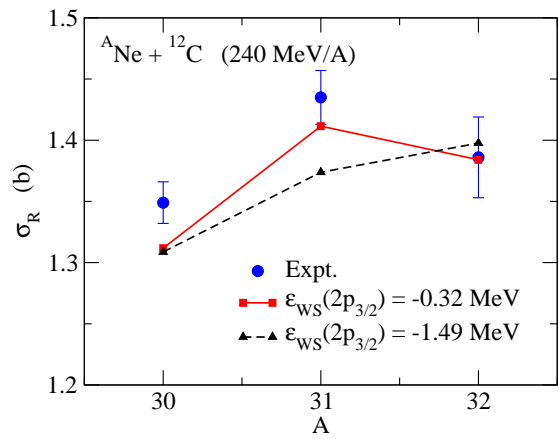


FIG. 3: (Color online) Reaction cross sections of Ne isotopes on a ^{12}C target at $E_{\text{lab}}=240$ MeV/A. The cross sections are calculated with the Glauber theory with HF and HFB densities. The solid line with the filled squares shows the results of $S_n(^{31}\text{Ne}) = |\epsilon(2p_{3/2})| = 0.32$ MeV, while the dashed line with the open triangles is obtained for $S_n(^{31}\text{Ne}) = |\epsilon(2p_{3/2})| = 1.49$ MeV. The experimental data are taken from Ref. [8].

to two different separation energies of the $2p_{3/2}$ neutron state. The dashed line with triangles is obtained using the wave functions with the separation energy $S_n(^{31}\text{Ne}) = |\epsilon_{\text{WS}}| = 1.49$ MeV, while the solid line with squares is calculated with the wave functions of $S_n(^{31}\text{Ne}) = |\epsilon_{\text{WS}}| = 0.32$ MeV. The empirical separation energy of ^{31}Ne has a large ambiguity with $S_n = 0.29 \pm 1.64$ MeV [25]. The cross section σ_R of ^{30}Ne is already much larger than the systematic values of Ne isotopes with $A < 30$. On top of that, we can see a clear odd-even staggering in the results with the smaller separation energy, $S_n = 0.32$ MeV, as much as in the experimental data, while almost no staggering is seen in the case of the larger separation energy, $S_n = 1.49$ MeV. This difference is easily understood by looking at the anti-halo effect for $|\epsilon_{\text{WS}}| \leq 1$ MeV shown in the middle panel of Fig. 2. Recently, the effect of deformation of neutron-rich Ne isotopes on reaction cross sections was evaluated using a deformed Woods-Saxon model [26]. It was shown that the deformation is large as much as $\beta_2 \sim 0.42$ in ^{31}Ne and enhances the reaction cross section by about 5%. However, the calculated results did not show any significant odd-even staggering in σ_R between ^{28}Ne and ^{32}Ne [26].

We mention that the pairing anti-halo effect may appear also in lighter halo nuclei. In Borromean systems, only the three-body system as a whole is bound and none of the two-body subsystems is unbound. In the case of ^{11}Li nucleus, this idea is implemented in that ^{11}Li is bound while ^{10}Li and a di-neutron are unbound. That is, the pairing correlations work in the continuum and gain the binding energy to make the three-body system bound [27, 28]. We can make a simple estimate on how large the anti-halo effect is in the ^{11}Li nucleus. The experimental

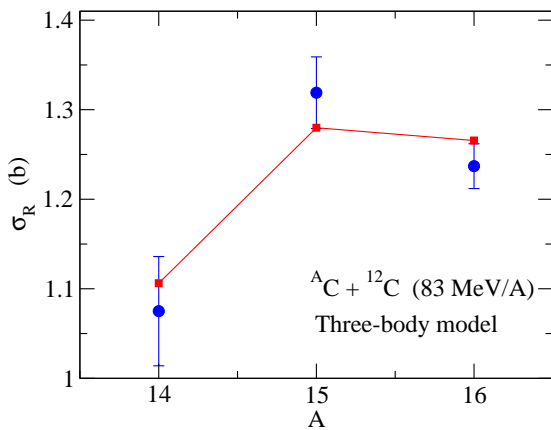


FIG. 4: (Color online) Reaction cross sections of C isotopes on a ^{12}C target at $E_{\text{lab}}=83$ MeV/A. The cross sections are calculated with the Glauber theory with three-body model densities. The experimental data are taken from Ref. [32].

matter radii were obtained for ^9Li and ^{11}Li as

$$\begin{aligned} \sqrt{\langle r^2 \rangle_m} &= 2.43 \pm 0.02 \text{ fm} \quad ^9\text{Li}, \\ \sqrt{\langle r^2 \rangle_m} &= 3.27 \pm 0.24 \text{ fm} \quad ^{11}\text{Li}, \end{aligned} \quad (8)$$

respectively[1]. The matter radius of the two neutrons outside the ^9Li core can be estimated by using a formula (see *e.g.*, Ref. [29]),

$$\langle r^2 \rangle_{2n} = \frac{11}{2} \left(\langle r^2 \rangle_m(^{11}\text{Li}) - \frac{9}{11} \langle r^2 \rangle_m(^9\text{Li}) \right) = (5.68)^2 \text{ fm}^2. \quad (9)$$

On the other hand, the rms radii of single particle states $1p_{1/2}$ and $2s_{1/2}$ could be calculated with a Woods-Saxon potential adjusting the separation energy as $S_n = |\epsilon_{\text{WS}}|=0.15$ MeV;

$$\begin{aligned} \sqrt{\langle r^2 \rangle} &= 6.48 \text{ fm} \quad \text{for } 1p_{1/2} \\ \sqrt{\langle r^2 \rangle} &= 10.89 \text{ fm} \quad \text{for } 2s_{1/2}. \end{aligned} \quad (10)$$

These values lead to the rms radius of ^{11}Li to be 3.53 fm and 5.14 fm assuming pure $(1p_{1/2})^2$ and $(2s_{1/2})^2$ two-neutron configurations outside the ^9Li core, respectively. These values are apparently larger than the empirical value, 3.27 fm, and thus one sees the pairing anti-halo effect in the matter radius of ^{11}Li .

The manifestation of the pairing anti-halo effect may be trivial for ^{11}Li as ^{10}Li is unbound. We therefore investigate next neutron-rich C isotopes. We particularly study the ^{16}C nucleus using a three-body model given in Ref. [30]. In this case, the valence neutron in ^{15}C occupies the $2s_{1/2}$ level at $\epsilon_{\text{WS}} = -1.21$ MeV, while ^{16}C is an admixture of mainly the $(2s_{1/2})^2$ and $(1d_{5/2})^2$ configurations. Assuming the set D given in Ref. [30] for the parameters of the Woods-Saxon and the density distribution for ^{14}C given in Ref. [31], the rms radii are estimated to be 2.53, 2.90, and 2.81 fm for ^{14}C , ^{15}C , and ^{16}C , respectively. The corresponding reaction cross sections σ_R calculated with the Glauber theory are shown in Fig. 4. The calculation well reproduces the experimental odd-even staggering of the reaction cross sections, that is a clear manifestation of the pairing anti-halo effect.

In summary, we have studied the mass radii of Ne isotopes with the Hartree-Fock (HF) and Hartree-Fock-Bogoliubov (HFB) methods with a Woods-Saxon potential. The reaction cross sections σ_R were calculated using the Glauber theory with these microscopic densities. We have shown that the empirical odd-even staggering in the reaction cross sections of neutron-rich Ne isotopes with the mass $A=30 \sim 32$ is well described by the HFB density and can be considered as a clear manifestation of the pairing anti-halo effect associated with a loosely-bound $2p_{3/2}$ wave function. The anti-halo effect was examined by the three-body model calculations also for ^{11}Li and ^{16}C . We argued that the observed mass radius of ^{11}Li can be considered as an evidence for the anti-halo effect. We have also shown that the experimental reaction cross sections of $^{14-16}\text{C}$ are well reproduced, confirming the anti-halo effect in these nuclei.

We point out that the odd-even staggering in reaction cross sections has been widely observed in a series of nuclei with small separation energies, such as $^{14-16}\text{C}$ [32], $^{18-20}\text{C}$ [3], $^{28-30}\text{Ne}$, $^{30-32}\text{Ne}$ [8] and $^{36-38}\text{Mg}$ [33]. Evidently, the pairing anti-halo effect is commonly seen in those weakly-bound nuclei near the drip line.

We would like to thank M. Takechi and H. Sakurai for fruitful discussions on experimental data, and C.A. Bertulani for useful discussions on the Glauber theory. This work was supported by the Japanese Ministry of Education, Culture, Sports, Science and Technology by Grant-in-Aid for Scientific Research under the program numbers (C) 22540262 and 20540277.

-
- [1] I. Tanihata *et al.*, Phys. Rev. Lett. **55**, 2676 (1985); Phys. Lett. **B206**, 592 (1988).
[2] W. Mittig *et al.*, Phys. Rev. Lett. **59**, 1889 (1987).
[3] A. Ozawa *et al.*, Nucl. Phys. **A691**, 599 (2001).
[4] M. Fukuda *et al.*, Phys. Lett. **B268**, 339 (1991).
[5] T. Minamizono *et al.*, Phys. Rev. Lett. **69**, 2058 (1992).
[6] K. Riisager, A.S. Jensen and P. Moller, Nucl. Phys. **A548**, 393 (1992).

- [7] H. Sagawa, Phys. Lett. **B286**, 7 (1992).
[8] M. Takechi *et al.*, Nucl. Phys. **A834**, 412c(2010), and private communication.
[9] T. Nakamura *et al.*, Phys. Rev. Lett. **103**, 262501 (2009).
[10] Y. Ogawa, K. Yabana, and Y. Suzuki, Nucl. Phys. **A543**, 722 (1992).
[11] A. Kohama, K. Iida, and K. Oyamatsu, Phys. Rev. **C78**, 061601(R) (2008).

- [12] K. Bennaceur, J. Dobaczewski and M. Ploszajczak, Phys. Lett. **B496**, 154 (2000).
- [13] A. Bohr and B.R. Mottelson, *Nuclear Structure* (Benjamin, Reading, MA, 1975), Vol. I.
- [14] D.M. Brink and R.A. Broglia, *Nuclear Superfluidity: Pairing in Finite Systems* (Cambridge University Press, Cambridge, England, 2005).
- [15] J. Dobaczewski *et al.*, Phys. Rev. **C53**, 2809 (1996).
- [16] I. Hamamoto, Phys. Rev. **C81**, 021304(R) (2010).
- [17] Y. Urata, K. Hagino, and H. Sagawa, Phys. Rev. **C83**, 041303(R) (2011).
- [18] W. Horiuchi, Y. Suzuki, P. Capel, and D. Baye, Phys. Rev. **C81**, 024606 (2010).
- [19] K. Hagino and H. Sagawa, Phys. Rev. **C72**, 044321 (2005).
- [20] M. Yamagami and Nguyen Van Giai, Phys. Rev. **C69**, 034301 (2004).
- [21] I. Hamamoto, Phys. Rev. **C71**, 037302 (2005).
- [22] B. Abu-Ibrahim and Y. Suzuki, Phys. Rev. **C62**, 034608 (2000).
- [23] B. Abu-Ibrahim *et al.*, Phys. Rev. **C77**, 034607 (2008).
- [24] C.A. Bertulani and H. Sagawa, Nucl. Phys. **A588**, 667 (1995).
- [25] B. Jurado *et al.*, Phys. Lett. **B649**, 43 (2007).
- [26] K. Minomo *et al.*, arXiv:1104.1856 [nucl-th].
- [27] G.F. Bertsch and H. Esbensen, Ann. Phys. (N.Y.) **209**, 327 (1991).
- [28] M.V. Zhukov *et al.*, Phys. Rep. **231**, 151 (1993).
- [29] H. Esbensen, K. Hagino, P. Mueller and H. Sagawa, Phys. Rev. **C76**, 024302 (2007).
- [30] K. Hagino and H. Sagawa, Phys. Rev. **C75**, 021301(R) (2007).
- [31] Yu. L. Parfenova, M.V. Zhukov, and J.S. Vaagen, Phys. Rev. **C62**, 044602 (2000).
- [32] D.Q. Fang *et al.*, Phys. Rev. **C69**, 034613 (2004).
- [33] M. Takechi, private communication.